Langmuir

ARTICLE

pubs.acs.org/Langmuir

Influence of Surface Hierarchy of Superhydrophobic Surfaces on Liquid Slip

Choongyeop Lee* and Chang-Jin "CJ" Kim

Mechanical and Aerospace Engineering Department, University of California, Los Angeles (UCLA), Los Angeles, California 90095, United States

ABSTRACT: We investigated how the surface hierarchy of superhydrophobic (SHPo) surfaces influences liquid slip by testing well-defined microposts that have nanoposts only on their top. Contrary to the commonly held belief, our results show that such hierarchical surfaces do not always lead to an increase of slip length despite their reduced solid fraction and enhanced hydrophobicity compared to single-scale surfaces. Adding nanoposts on top of the microposts resulted in an increase of slip length only if the original microposts had a solid fraction above a threshold value. For solid fractions below this threshold, adding nanoposts decreased the slip length. We propose that there were not enough nanoposts on the top surface of very thin microposts to support the liquid pressure, allowing the liquid to intrude down to the top corners of the microposts.

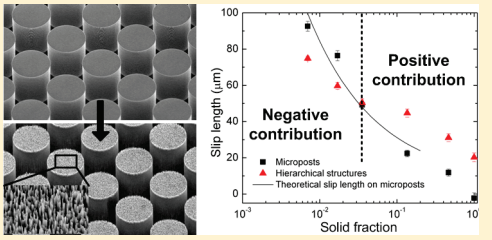

INTRODUCTION

A liquid droplet moving (sliding/rolling) on a structured surface in the dewetted (or Cassie−Baxter) state, or a superhydrophobic (SHPo) surface, experiences far less resistance (e.g., even by over 99%[1]) than it would on a flat surface of the same material. Similarly, a bulk liquid can also move (flow) with less resistance, because the gas in between the structures produces an effective slip.[2] The amount of slip is best quantified by "slip length", that is, the ratio of liquid velocity to shear rate at the wall. Although much larger than the intrinsic slip on smooth surfaces (slip length on the order of 10 nm), the typical effective slips on structured surfaces achieved in recent years (even those above 10 μm[3,4]) are still so small that their manifestation has been limited to microchannels[3−6] or surface phenomena.[7] To have any impact on macroscale systems (e.g., vessels, pipe flows), much larger slip lengths (over 100 μm[8,9]) are needed.

The amount of slip was theoretically[10−17] and experimentally[4,8,9,19] shown to depend on various parameters of a SHPo surface as well as how confined the liquid flow is.[14,15,18] For example, in addition to the primary parameters, that is, a solid fraction and a structural pitch of surface patterns, a slip length also depends on the secondary parameters, such as an intrinsic slip on the solid−liquid interface[10,12,15] and a finite slip on a liquid−gas interface.[10,12,17,18] Also, under a confined condition (e.g., channel height ≪ structural pitch), a slip length is strongly influenced by the channel height.[14,15,18] However, the contribution of the secondary effects to the overall slip is expected negligible if slips by the secondary effects are too small (~20 nm on hydrophobic surface) or too large (more than millimeters at water−air interface) compared to slips on microstructures (tens[3,4] to a hundred[8,9] micrometers). For the confinement effect, as long as surface microstructures have much smaller scale than the channel height, the channel size does not influence the slip length. Ignoring the secondary effects, one may view that the slip length increases linearly with a pitch and rapidly with a gas fraction.[8,12,16]

Meanwhile, the influence of a surface hierarchy on superhydrophobicity was intensively investigated in recent years, inspired by the hierarchical structures found on many natural SHPo surfaces (e.g., lotus leaves).[20,21] It has been found that a surface hierarchy not only enhances the hydrophobicity of a surface,[22−25] but also renders a SHPo surface more robust to the Cassie-to-Wenzel wetting transition.[9,25,26] This robustness allowed surfaces with a larger pitch for slip experiments (i.e., staying dewet), resulting in the slip length as high as 400 μm.[9] However, the increase was an indirect result of surface hierarchy, because the roughness was added only to the side surface of the structures and not in contact with the flowing liquid. A question remains how the roughness added to the top surface of the structures will affect the slip. While many claimed surface hierarchy would increase the slip and drag reduction, there has never been a clear description with supporting experiments, perhaps because it is challenging to fabricate hierarchical SHPo surfaces of controlled geometries and those with which the effect of the second-scale structures (i.e., added roughness) can be isolated. Considering the various advantages hierarchical surfaces have over single-scale surfaces regarding superhydrophobicity, it is important to understand how a surface hierarchy affects the slip length. This knowledge will help include hierarchical structures in the design of hydrophobic surfaces for applications involving a continuous liquid flow.

Received: November 1, 2010
Revised: February 8, 2011
Published: March 03, 2011

EXPERIMENTAL DETAILS

Sample Preparation. To quantify the effect of surface hierarchy, the slip length on each length scale (i.e., nanoscale and microscale) needs to be quantified first. Normally, the slip length on nanostructured surfaces is expected to be very small due to their small pitches,[6] requiring high-precision measurement techniques. However, if a solid fraction on such nanostructures can be engineered to be very low (e.g., below 0.1%), it is possible to achieve a slip length several times the pitch of nanostructures,[4] allowing the use of less accurate but more convenient methods (e.g., rheometer[4]) for slip measurements. Therefore, our goal is to construct hierarchical SHPo surfaces in a way that nanostructures of a very low solid fraction are made on top of microstructures, so that the change of slip length by the added nanostructures is clearly distinguishable by the rheometer measurement.

To prepare such hierarchical SHPo surfaces, we first fabricated microposts with a fixed pitch of 50 μm and varying target solid fractions of 1, 2, 5, 15, and 50% on a 60 mm diameter circular area on a 100 mm diameter silicon wafer by using a specialized photolithography developed in-house for defect-free samples[8] and deep reactive ion etching (DRIE). The pitch and solid fraction of microposts were decided based on the consideration that they should be sufficiently large and small, respectively, to ensure that the expected slip lengths on microposts are much larger than the accuracy of the measurement system ($\sim$7 μm[27]) but not too large to result in Cassie-to-Wenzel transition during our slip measurements, which have a working pressure of 200−300 Pa. The height of the microposts on all the samples was maintained to be 50 μm, which was large enough to ensure that the liquid−gas meniscus did not touch the bottom surface of the microposts due to the sagging.[4]

After the fabrication, actual solid fractions were determined from scanning electron microscopy (SEM) images, which turned out to be 0.7, 1.7, 3.5, 13.6, and 46.6%, respectively. To add surface hierarchy to microposts, an additional DRIE process with a modified recipe was performed for 40 min on each sample to generate random nanoposts ("black silicon method"[1,4]) on top of the microposts. The SEM images of the resultant structures without and with nanostructuring are shown in Figure 1, panels a and b, respectively. The magnified image of nanoposts above Figure 1b shows that sharp nanoneedles were randomly formed with a pitch of 0.5−1 μm on a silicon surface. Also, Figure 1a,b confirms that the nanoposts were successfully formed without compromising the overall geometry of microposts. Because of the random nature of the black silicon method, the height of the nanoposts was observed to vary between samples. Still, the pitch of nanoposts (0.5−1 μm) and their sharp tips were observed to be similar in every sample, implying that the process variation between DRIE runs would not distort our results, since a slip length depends mainly on a pitch and a solid fraction but not on a height. Finally, each sample was treated to be hydrophobic with 1H,1H,2H,2H-perfluorodecyltrichlorosilane (FDTS) (96%, Lancaster Synthesis, Inc.) by placing the sample inside 0.1 M FDTS solution in 2,2,4-trimethylpentane (99.8%, Aldrich) under the nitrogen environment for 10 min. FDTS was chosen as a hydrophobic coating, as its molecularly thin layer ($\sim$1.4 nm[28]) would not modify the morphology of surface structures.

Slip Measurements. To measure slip lengths, we used a cone-and-plate rheometer for its easy implementation, which provides accuracy better than 7 μm (typically 2−3 μm).[8,27] Deionized water was used as the test liquid, and the temperature during the measurement was maintained at 25 °C by a Peltier plate. Please note that we checked the accuracy of the rheometer system on a flat surface by varying the temperature (i.e., in a range of the measured torque), confirming that 7 μm accuracy was preserved up to the temperature of 30 °C.

Since the slip length of about 20 μm was obtained on nanoposts fabricated by the same black silicon method,[4] the use of a rheometer was deemed acceptable in the present study. In the rheometry system, the truncation gap between a cone and a sample in the middle was 53 μm, and the cone angle was 2°, resulting in a gap size of $\sim$1 mm along the peripheral edge. The measured torque by rheometry was converted to a slip length using the mathematical relationship derived for the geometry.[8] The confinement effect was considered to be negligible in the present study, as the gap was much larger than the structural pitch of microposts (50 μm) on most area and the shear stress on regions farther from the center (corresponding to a larger gap) would dominate the measured torque (i.e., slip length). For example, the area with the gap below 500 μm (i.e., gap/pitch = 10) accounted for only $\sim$10% of the measured torque. Therefore, it is reasonable to assume that a slip length depended only on surface structures and was not affected by the details of global flow configuration.

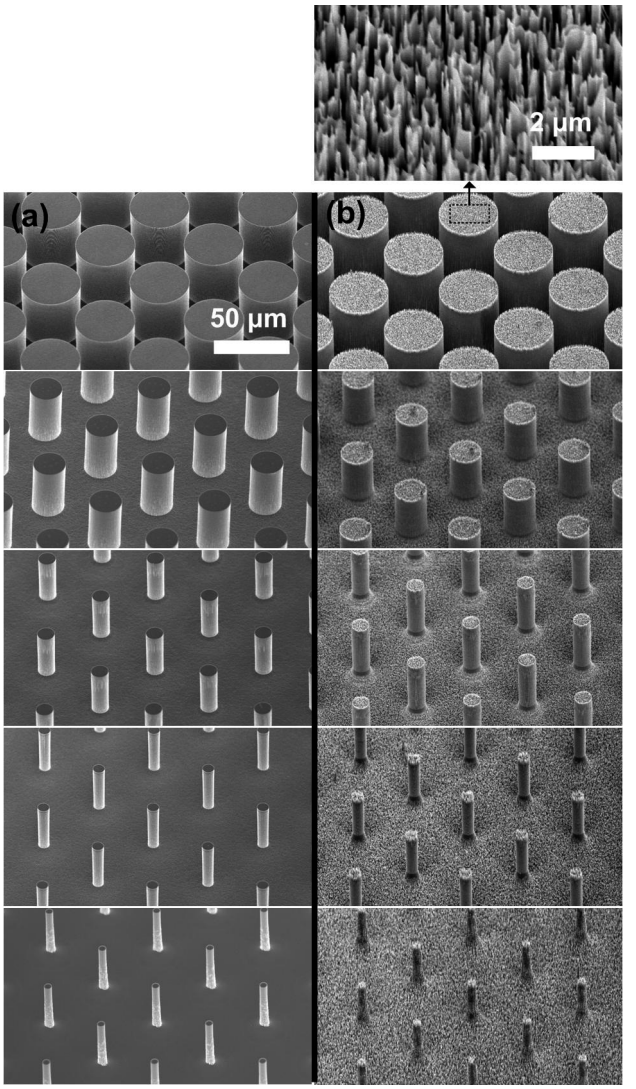

Figure 1. (a) Scanning electron microscopy (SEM) images of microposts with 50 μm pitch and target solid fractions of 50, 15, 5, 2, and 1% (top → bottom). (b) SEM images of corresponding hierarchical structures, whose horizontal surfaces consist of nanoposts generated by a black silicon method. A magnified picture (inset) shows the nanoposts on the top surface of a micropost.

RESULTS AND DISCUSSION

Figure 2a shows the measured slip lengths on hierarchical structures δ_{hier} along with the theoretical and measured slip

dx.doi.org/10.1021/la104368v |*Langmuir* 2011, 27, 4243–4248

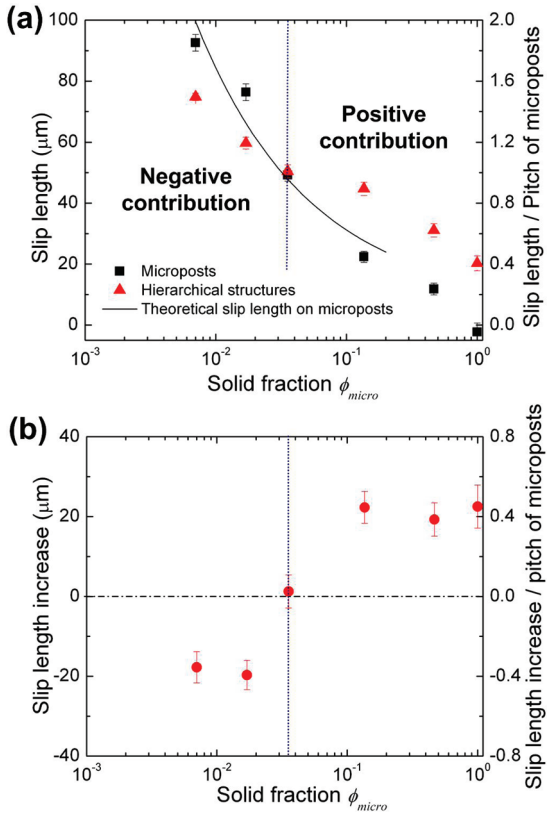

Figure 2. The effect of nanoposts added on top of microposts on the overall slip. (a) The measured slip lengths on hierarchical posts as a function of the (original) solid fraction of microposts ϕ_{micro} along with the measured[8] and theoretical[12] slip lengths on single-scale microposts. (b) Increase in the measured slip length. The slip lengths on hierarchical posts are measured to be higher than those on single-scale microposts by a constant amount down to solid fraction of around 10%, below which the trend is reversed.

lengths on microposts δ_{micro} for comparison. In this graph, x-axis denotes an original (i.e., single scale) solid fraction of microposts ϕ_{micro}. For hierarchical structures, this will denote a solid fraction before nanostructuring, not the actual (eventual) solid fraction. If a solid fraction of nanoposts is ϕ_{nano}, the actual solid fraction of hierarchical posts ϕ_{hier} will be $\phi_{micro}\phi_{nano}$. When compared with microposts, slip lengths on hierarchical posts are consistently larger (by ~20 μm) as expected, but only up to a point. The difference starts to decrease when ϕ_{micro} decreases below 10%, and eventually the slip length on hierarchical posts drops even below that of microposts. This unexpected result challenges the general conception that a decreased overall solid fraction on hierarchical posts will lead to a larger slip length. The difference of slip lengths on hierarchical posts relative to microposts is depicted in Figure 2b, which provides a clear trend of slip length change by the secondary structures as a function of ϕ_{micro}.

Although there have been several theoretical or numerical studies investigating the effect of a finite slip on solid patches,[10,12,15,29] we followed the scaling law by Ybert et al.[12] to explain the change of slip lengths on hierarchical structures due to the geometrical similarity (i.e., posts). Furthermore, the validity of this scaling law was verified on circular posts in the entire range of the solid fraction in Ng and Wang.[29] According to the scaling law, an additional increase of overall slip length due to an intrinsic slip δ_0 on the top surface of the posts, relative to the

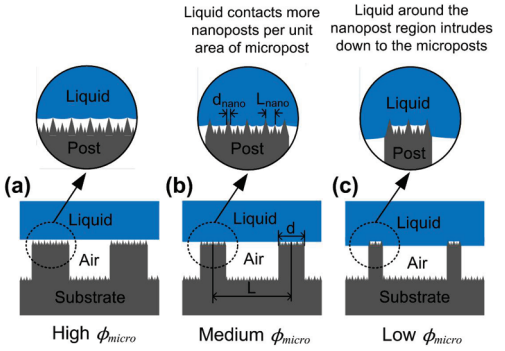

Figure 3. Schematic representation of the interface between a liquid and a hierarchical SHPo surface for a given liquid pressure, as the solid fraction of the microposts ϕ_{micro} decreases. (a) Initially, the liquid touches only some of the nanoposts (taller ones). (b) As ϕ_{micro} decreases (i.e., the microposts become thinner), the number of nanoposts per overall sample area decreases. As a result, the solid−liquid−air triple line moves down slightly (very roughly by 0−0.5 μm in Figure 1b inset) to contact more nanoposts. The shorter nanoposts newly contacting the liquid help overcome the reduced number of total nanoposts. (c) Below a threshold ϕ_{micro}, after the triple line contacted many of the nanoposts, it slides down the sidewalls of the outer nanoposts on the corner of each micropost to their foot level (very roughly by 3 μm in Figure 1b inset), where the surface tension force increases significantly because the full perimeter (corner) of a micropost is added to the total contact length of the interface. Note the liquid intrusion occurred without Cassie-to-Wenzel transition on the nanoposts.

case with no intrinsic slip on the top surface of the posts, is expected as follows

$$\Delta\delta = \frac{c_1\delta_0}{\phi_{micro}} = \frac{4c_1L^2\delta_0}{\pi d^2} \quad (1)$$

where L and d are the pitch and diameter of microposts, respectively, and c_1 is proportionality constant (i.e., 1.006−1.048[29]). In the presence of nanoposts on top, we assume that the intrinsic slip can be replaced by the effective slip on nanoposts derived also by the scaling law[13]

$$\delta_0 = \frac{c_2L_{nano}}{\sqrt{\phi_{nano}}} = \frac{2c_2(L_{nano})^2}{\sqrt{\pi}d_{nano}} \quad (2)$$

where L_{nano} is the pitch of nanoposts, d_{nano} is a diameter (at the contact line) of nanoposts, and c_2 is a proportionality constant. The exact value of c_2 on a square array of posts was analytically calculated in Davis and Lauga[16] and was shown to be 0.332, close to the 0.325 in Ybert et al.[12] However, in the rhoemetry system the flow was not always aligned with the periodicity of posts, leading to a smaller proportionality constant of c_2 = 0.1555 in our previous study.[9]

Since nanoposts consist of sharp needles of varying heights (Figure 3a), a liquid is expected to touch only taller nanoposts under a low liquid pressure. However, if the pressure increases, the liquid will move down slightly to contact more nanoposts (the wetted area of each nanopost also increases), so that there are enough contacts to sustain the pressure. Note that the maximum supporting force a surface tension can provide before the liquid−solid−air contact line slides down is proportional to the total length of the contact lines on which the surface tension can act. While well described by an energy consideration,[30] the above aspect was missed in the force consideration of Choi and

dx.doi.org/10.1021/la104368v |Langmuir 2011, 27, 4243–4248

Kim,[4] where a one-dimensional force balance, valid only for grates, was applied to the posts.

Although the liquid pressure does not increase in our slip tests, a similar effect arises when the solid fraction of microposts ϕ_{micro} becomes small. As the microposts become thinner, the top area of a micropost decreases, resulting in a smaller total number of nanoposts on a given overall sample area. To overcome the fewer nanoposts against the same liquid pressure, more of the existing nanoposts should contact the liquid and also each nanopost should provide more wetted area (more contact line), which makes the liquid moving down from the original level (Figure 3b). For each cell with one period of posts ($L \times L$), a force by the liquid pressure is given by $L^2\Delta P$, while the supporting force by surface tension is given by $-L^2\phi_{micro}\gamma n d_{nano} \cos\theta$. Here, ΔP is the differential pressure of liquid over air, $L^2\phi_{micro}$ is the top surface area of microposts where nanoposts are populated, and n is the number of nanoposts contacting the liquid per unit area of micropost top surface ($n = 1/L_{nano}{}^2$). Each nanopost on the microposts contributes to the supporting force by $-\gamma d_{nano} \cos\theta$, where θ is the contact angle and ΔP is the differential pressure of liquid over air. These two conditions can be estimated with the following force balance

$$L^2\Delta P = -L^2\phi_{micro}\gamma n d_{nano}\cos\theta = \frac{-\pi d^2\gamma n d_{nano}\cos\theta}{4} \quad (3)$$

Equation 3 constitutes a basic relationship between the surface parameters of nanoposts and those of microposts on hierarchical posts. Please note that the change of θ with ΔP has been predicted in theoretically[33] and experimentally demonstrated.[3]

When eq 3 is plugged into eq 2, the following equation is derived

$$\delta_0 = \frac{-c_2\sqrt{\pi}\left(\frac{d^2}{L^2}\right)\left(\frac{\gamma}{\Delta P}\right)\cos\theta}{2} \quad (4)$$

Equation 4 states that the slip length of the nanoposts will decrease as a result of the increased contact area between the liquid and nanoposts if the liquid pressure increases or the solid fraction of the microposts (d^2/L^2) decreases. Then, the increase of the slip length on the hierarchical posts relative to the microposts is obtained from eqs 1 and 4 as follows

$$\Delta\delta = \frac{4c_1\left(\frac{L}{d}\right)^2\delta_0}{\pi} = \frac{-2c_1c_2\left(\frac{L}{d}\right)^2\left(\frac{d}{L}\right)^2\left(\frac{\gamma}{\Delta P}\right)\cos\theta}{\sqrt{\pi}} = \frac{-2c_1c_2\left(\frac{\gamma}{\Delta P}\right)\cos\theta}{\sqrt{\pi}} \quad (5)$$

Equation 5 implies that the slip increase due to the irregular nanoposts on top of the microposts would be independent of the surface parameters of the microposts (i.e., L and ϕ_{micro}) and the expected slip increase in the present experimental conditions (γ = 0.072 N/m for water at 25 °C, ΔP = 200−300 Pa) would be 21−33 μm, which is in accord with our observation for ϕ_{micro} down to 0.136 (Figure 2).

Our results suggest that any attempt to increase a slip through a surface hierarchy will be strongly limited by the liquid pressure due to the stability condition for the dewetted state. Also, the amount of the slip increase would be independent of any details of surface microstructures, provided the liquid pressure can be sustained by nanostructures alone. However, the increase vanished at ϕ_{micro} = 0.035. Below this length, the trend was reversed (for ϕ_{micro} = 0.017 and 0.007), that is, the overall slip became smaller than that on the microposts only. To explain the deviation from the common expectation when the solid fraction of microposts is very low, we present the following discussion.

As long as there is a positive slip on the top surface of the microposts, the overall slip length on hierarchical posts should always increase from that on microposts, according to eq 1. If the nanoposts become wetted, they may incur a negative slip (i.e., defined from the top surface of the micropost) on the top surface of the micropost, causing a decrease in the overall slip length. However, our hierarchical structures exhibited no adhesion with the liquid both before and after testing, excluding any possibility of wetting. Instead, we suspect additional dissipation by the liquid intrusion was the culprit for the decreased overall slip on the hierarchical structures of very low ϕ_{micro}. At very low ϕ_{micro}, there is not enough support from nanoposts to sustain a liquid pressure, as the total number of nanoposts decreases. With the support from nanoposts insufficient, the contact angle on the sidewall increases (i.e., the liquid−gas meniscus curves more), or the solid−liquid−gas triple line slides down the nanoposts, which are thicker at the bottom. Although both mechanisms (meniscus curving and triple-line sliding) can effectively decrease the overall slip length by incurring additional dissipation,[13,31−34] we suspect that the observed decrease of slip length resulted more likely from the downward sliding of the triple line for two reasons. First, the contact angles on the sidewall of both microposts and hierarchical structures would be limited between 90 and 120°. Even if there is a difference in the actual contact angle on the sidewall between the two cases, their difference is too small (less than 30°) to impart any significant difference in slip length by the curvature difference. Second, the decrease of slip lengths by a meniscus curvature was shown to be more gradual compared to the decrease by the downward sliding of the triple line.[34] For example, on grates transverse to a liquid flow with a solid fraction of 10%, 20% decrease in the slip length required a contact angle change from 90 to 180° on the sidewall.[34] Meanwhile, the same amount of slip decrease is expected for a liquid intrusion amounting to several percentages of a pitch (∼a few micrometers). Furthermore, the slip decrease by the triple-line sliding becomes more significant at a low solid fraction and in the presence of additional slips on top of solids,[33] similar to our experimental conditions. In these conditions, a triple-line sliding even below 1 μm can significantly decrease the slip length.

On hierarchical structures, the downward sliding of the triple line can happen when the energy cost to move the liquid farther down in between the nanoposts (i.e., wet the nanoposts) becomes more than that needed to move the liquid outside of the nanopost region down until the contact line reaches the foot of nanoposts and the top corner of the micropost (Figure 3c). From a force balance, the condition for the downward sliding of the triple line can be expressed as follows

$$\frac{d}{\left(\frac{L^2-\pi d^2}{4}\right)} < \frac{d_{nano}}{\left(\frac{L_{nano}^2-\pi d_{nano}^2}{4}\right)} \quad (6)$$

On microposts with L = 50 μm and ϕ_{micro} = 5%, for example, the liquid will slide down the microposts if the liquid pressure is larger than 600 Pa.[8] If the surface is made hierarchical by adding 1 μm pitch nanoposts (for example) on top of the microposts, eq 6

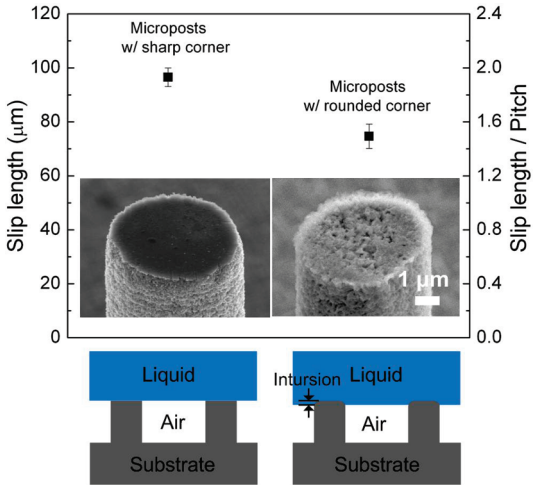

Figure 4. The decrease of slip lengths on microposts (50 μm pitch and 1% target solid fraction) when top corners are rounded. The insets show SEM images of micropost with a sharp (left)[9] and a rounded (right) top corner. Schematics illustrate how a rounded top corner may promote the liquid intrusion by an amount comparable to the radius of curvature, which is ~0.1 μm in the given round-cornered (right) micropost.

indicates that the liquid will slide down microposts once it wets the top portion of the nanoposts below 5 nm in diameter at 600 Pa. When the hierarchical surface can resist the liquid pressure with the nanoposts alone (Figure 3a,b), the slip on the nanoposts makes the overall slip increase. However, if the micropost has to participate to resist the liquid pressure because there are not enough nanoposts at a very low ϕ_{micro} (Figure 3c), the negative effect of the downward sliding of the triple line may outweigh the positive effect of the nanoposts.

The effect of the downward sliding of the triple line on slip is further corroborated by a separate experiment on microposts of a sharp and a rounded top corner, fabricated by the method described in Lee and Kim[9] and summarized in Figure 4. The sharp-cornered microposts were prepared by forming nanostructures only on the sidewall surfaces,[9] while the round-cornered microposts were by forming nanostructures everywhere. An ideal sample would feature round-cornered microposts with nanostructures only on the sidewall surfaces, which could not be fabricated, unfortunately. Fortunately, however, the effect of the top nanostructures on the overall slip length is negligible due to their small pitch (20−30 nm). This leaves the roundness of the corners as the only difference between the two samples that may influence the overall slip. When all other parameters that affect the slip length are kept the same (L = 50 μm; ϕ_{micro}= 1%), the microposts with a sharp corner exhibited a slip length (89.8 μm) unmistakably larger than those with a rounded corner did (73.4 μm). We reason the reduction of the slip on the rounded corners as follows. For the case of sharp corners, the solid−liquid−gas triple line remains at the corner when the liquid−gas meniscus curves downward by the liquid pressure. For the case of rounded corners, on the other hand, the triple line starts to slide down along the gradual corner, that is, below the horizontal plane of the posts' top, in addition to the meniscus curving by the pressure. While the intrusion accounted by the meniscus curvature is similar for both the cases, the intrusion by the downward sliding of the triple line exists only for the case of rounded corners. Note the body of liquid between the horizontal plane of the posts' top and the horizontal plane of the triple lines. Although the amount of this sliding is small, less than the radius of the rounded corner (~0.1 μm), its negative effect to the slip length is noticeable, as demonstrated by several numerical studies.[31−34] Incidentally, note that the sharp-corner sample in Figure 4 has a surface morphology (i.e., nanoporous surface on only on the side of the posts[9]) different from what the sample in Figure 2 has (i.e., needlelike nanoposts[1,4] only on the top of the posts), so their slip lengths should not be expected the same despite the identical pitch and solid fraction of their microposts.

CONCLUSION

We have observed an increase of slip on hierarchical structures relative to that on microstructures. Furthermore, the amount of the increase in slip length was not dependent on the solid fraction of the microstructures. However, the nanostructures added to make the structures hierarchical led to a decrease of slip if the original microstructures already had a very small solid fraction (below 10%), imposing a limit to the commonly held belief that the decrease in the overall solid fraction by the surface hierarchy will increase the slip. Although the slip on nanostructures indeed helps increasing the overall slip length on hierarchical structures, the negative effect of downward sliding of the solid−liquid−gas triple line into microstructures at a low solid fraction of the microstructures may overshadow the positive effect of the nanostructures. Our findings help explain the discrepancy among the reported slip data in other experimental studies. On polymer microstructures (e.g., PDMS), for instance, the roundness of corners, expected for molded polymer structures, will adversely affect the slip length, yielding a smaller slip length than theoretically predicted.[35] In comparison, slip lengths on silicon microstructures agreed well with the theories due to their sharp corners that do not allow the downward sliding of the triple line.[8,9] We believe that our findings help clarifying the roles and limitations of secondary roughness on hierarchical SHPo surfaces for the slip and drag reduction of liquid flows.

AUTHOR INFORMATION

Corresponding Author

*Tel: 1-310-825-3977. Fax: 1-213-206-2302. E-mail: choongyeop@ucla.edu.

ACKNOWLEDGMENT

This research has been funded by the National Science Foundation NIRT Grant 0103562 and California NanoSystems Institute (CNSI) Graduate Student Fellowship. The authors thank Professor Pirouz Kavehpour for the access to the rheometer.

REFERENCES

(1) Kim, J.; Kim, C.-J. *Proceedings of the 15th IEEE International Conference on Micro Electro Mechanical System*; IEEE: Piscataway, NJ, 2002; pp 479−482.
(2) Philip, J. R. *J. Appl. Math. Phys. (ZAMP)* **1972**, *23*, 353–372.
(3) Ou, J.; Perot, B.; Rothstein, J. P. *Phys. Fluids* **2004**, *16*, 4635–4643.
(4) Choi, C.-H.; Kim, C.-J. *Phys. Rev. Lett.* **2006**, *96*, 066001.
(5) Rothstein, J. P. *Annu. Rev. Fluid Mech.* **2010**, *42*, 89–109.
(6) Choi, C.-H.; Ulmanella, U.; Ho, C.-M.; Kim, C.-J. *Phys. Fluids* **2006**, *18*, 087105.

(7) Huang, D. M.; Cottin-Bizonne, C.; Ybert, C.; Bocquet, L. *Phys. Rev. Lett.* **2008**, *101*, 064503.
(8) Lee, C.; Choi, C.-H.; Kim, C.-J. *Phys. Rev. Lett.* **2008**, *101*, 064501.
(9) Lee, C.; Kim, C.-J. *Langmuir* **2009**, *25*, 12812–12818.
(10) Cottin-Bizonne, C.; Barentin, C.; Charlaix, E.; Bocquet, L.; Barrat, J.-L. *Eur. Phys. J. E* **2004**, *15*, 427–438.
(11) Priezjev, N. V.; Darhuber, A. A.; Troian, S. M. *Phys. Rev. E* **2005**, *71*, 041608.
(12) Ybert, C.; Barentin, C.; Cottin-Bizonne, C.; Joseph, P.; Bocquet, L. *Phys. Fluids* **2007**, *19*, 123601.
(13) Sbragaglia, M.; Prosperetti, A. *Phys. Fluids* **2007**, *19*, 043603.
(14) Bocquet, L.; Barrat, J.-L. *Soft Matter* **2007**, *3*, 685–693.
(15) Feuillebois, F.; Bazant, M. Z.; Vinogradova, O. I. *Phys. Rev. Lett.* **2009**, *102*, 026001.
(16) Davis, A. M. J.; Lauga, E. J. *Fluid Mech.* **2010**, *661*, 402–411.
(17) Belyaev, A. V.; Vinogradova, O. I. J. *Fluid Mech.* **2010**, *652*, 489–499.
(18) Belyaev, A. V.; Vinogradova, O. I. *Soft Matter* **2010**, *6*, 4563–4570.
(19) Joseph, P.; Cottin-Bizonne, C.; Benoit, J.-M.; Ybert, C.; Journet, C.; Tabeling, P.; Bocquet, L. *Phys. Rev. Lett.* **2006**, *97*, 156104.
(20) Barthlott, W.; Neinhuis, C. *Planta* **1997**, *202*, 1–8.
(21) Koch, K.; Bohn, H. F.; Barthlott, W. *Langmuir* **2009**, *25*, 14116–14120.
(22) Cheng, Y. T.; Rodak, D. E.; Wang, C. A.; Hayden, C. A. *Nanotechnology* **2006**, *17*, 1359–1362.
(23) Zhu, L.; Xiu, Y.; Xu, J.; Tamirisa, P. A.; Hess, D. W.; Wong, C.-P. *Langmuir* **2005**, *21*, 11208–11212.
(24) Gao, X.; Yao, X.; Jiang, L. *Langmuir* **2007**, *23*, 4886–4891.
(25) Jeong, H. E.; Kwak, R.; Kim, J. K.; Suh, K. Y. *Small* **2008**, *4*, 1913–1918.
(26) Kwon, Y.; Patankar, N.; Choi, J.; Lee, J. *Langmuir* **2009**, *25*, 6129–6136.
(27) Choi, C.-H.; Kim, C.-J. *Phys. Rev. Lett.* **2006**, *97*, 109602.
(28) Maboudian, R.; Ashurst, W. R.; Carraro, C. *Sens. Actuators* **2000**, *82*, 219–223.
(29) Ng, C.-O.; Wang, C. Y. *Microfluid. Nanofluid.* **2010**, *8*, 361–371.
(30) Barbieri, L.; Wagner, E.; Hoffmann, P. *Langmuir* **2007**, *23*, 1723–1734.
(31) Biben, T.; Joly, L. *Phys. Rev. Lett.* **2008**, *100*, 186103.
(32) Joly, L.; Biben, T. *Soft Matter* **2009**, *5*, 2549–2557.
(33) Ng., C.-O.; Wang, C. Y. *Phys. Fluids* **2009**, *21*, 013602.
(34) Teo, C. J.; Khoo, B. C. *Microfluid. Nanofluid.* **2010**, *9*, 499–511.
(35) Tsai, P.; Peters, A. M.; Pirat, C.; Wessling, M.; Lammertink, R. G. H.; Lohse, D. *Phys. Fluids* **2009**, *21*, 112002.